COBEM 2023 27TH INTERNATIONAL CONGRESS OF MECHANICAL ENGENEERING

ABCM Brazilian Society of Mechanical Sciences and Engineering
27th ABCM International Congress of Mechanical Engineering
December 04-08, 2023, Florianópolis-SC, Brazil

COB-2023-0832
A NEW FAMILY OF AUXETIC METAMATERIAL FOR SANDWICH BEAMS: THE ELLIPTICAL S-CHIRAL DESIGN INVESTIGATION

Nathalia Mello M. P.
Universidade Federal de Minas Gerais, Mechanical Engineering Graduate Studies Program, 6627 Antônio Carlos Avenue, Belo Horizonte, MG 31270-901, Brazil
Centro Federal de Educação Tecnológica de Minas Gerais, 5253 Amazonas Avenue, Belo Horizonte, MG 30421-190 Brazil
nathaliamello@ufmg.br and nathaliamello@cefetmg.br

Paulo C. M. Rodrigues
Universidade Federal de Minas Gerais, Department of Mechanical Engineering, 6627 Antônio Carlos Avenue, Belo Horizonte, MG 31270-901, Brazil
paulocmr@demec.ufmg.br

Alexandre S. Scari
Universidade Federal de Minas Gerais, Department of Mechanical Engineering, 6627 Antônio Carlos Avenue, Belo Horizonte, MG 31270-901, Brazil
scari@demec.ufmg.br

Almir Silva Neto
Centro Federal de Educação Tecnológica de Minas Gerais, Campus Timóteo, 121 Dezenove de Novembro Street, Timóteo, MG 35180-008, Brazil
almir.sneto@cefetmg.br

Antonio A. T. Maia
Universidade Federal de Minas Gerais, Department of Mechanical Engineering, 6627 Antônio Carlos Avenue, Belo Horizonte, MG 31270-901, Brazil
aamaia@demec.ufmg.br

Lazaro V. Donadon
Universidade Federal de Minas Gerais, Department of Mechanical Engineering, 6627 Antônio Carlos Avenue, Belo Horizonte, MG 31270-901, Brazil
lazaro@demec.ufmg.br

Antonio F. Ávila
Universidade Federal de Minas Gerais, Department of Mechanical Engineering, 6627 Antônio Carlos Avenue, Belo Horizonte, MG 31270-901, Brazil
avila@ufmg.br

Abstract. *Auxetic metamaterials are man-made materials displaying a negative Poisson Ratio. The chiral metamaterials can support larger overall strains than the classic re-entrant auxetic shape. Thus, the objective of this work was to obtain the flexural elastic properties of a family of sandwich beams with a chiral elliptical S-shaped core. To reach the objectives of this work, finite element simulations were obtained and an experimental setup with a sandwich beam made of a circular S-shaped core was performed. The experimental results were compared to the simulated ones in order to validate the simulations. The experimental samples were fabricated using additive manufacturing with polyacid lactic as raw material. An increase in the aspect ratio (a/b) of the ellipse core led to an increase in sandwich beam flexural stiffness and a reduction in mass. Moreover, the highest value of the core shear modulus was achieved with the (a/b) ratio around 1.5, followed by a decrease as the aspect ratio increased. This seemingly paradoxical finding, where sandwich beam flexural stiffness increased while the core shear modulus decreased, can be explained by the design's contribution to increasing the core's moment of inertia. Additionally, normal stress profiles in the x-direction did not differ significantly between the structures.*

Keywords: *metastructures, sandwich composite beams, auxetic materials, finite element method, additive manufacturing.*

1. INTRODUCTION

Mechanical meta-materials are man-made materials with properties not usually found in Nature (Liu and Zhang, 2011). Master and Evans (1996) defined auxetic meta-materials as a class of material with negative Poisson Ratio. Master and Evans auxetic model was based on the re-entrant unit cell derived from the honeycomb shape. Since the early days of meta-materials, different configurations were proposed and innumerous analytical and numerical models were created. As described by Francisco *et al*. (2022), the concept of auxetic behavior has countless applications, e.g., impact energy and vibration absorption. The "original" model proposed by Masters and Evans, however, has a limitation, the stress concentration around the edges (Masters and Evans, 1996). By changing these regions, Wang *et al*. (2018) were able to obtain a more uniform stress around each element of the re-entrant unit cell. Similar approach was developed by Zhang *et al*. (2020). Unfortunately, due to geometric limitations, the auxetic behavior based on re-entrant unit models is limited to mid-range deformations. To be able to solve this problem, a new class of auxetic material was proposed. Alderson *et al*. (2010) defined the so-called chiral configuration. They described three different families of chiral meta-structures, i.e., the hexachiral, the tetrachiral and the trichiral. In all cases, the negative Poisson Ratio condition was observed. Mousanezhad *et al*. (2016) went further by suggesting the anti-chiral geometric configuration. As commented by Montgomery-Liljeroth *et al*. (2023), the chiral geometry formulation and its variations have the advantage of keeping the negative Poisson ratio in a much larger deformation range. This is due to their favorable "empty" spaces and low density, which is not the case of the auxetic geometric formulation defined by the re-entrant model. In all cases, analytical models for predicting the elastic properties were proposed. Unfortunately, as discussed by Zhang *et al*. (2022), due to manufacturing constraints, it was only recently, with the additive manufacturing advances, that physical experiments were performed. As commented by Shukla and Behera (2022), a large number of comparative studies between experimental data from physical models created by additive manufacturing and numerical models were developed in recent years. The advantage of numerical simulations based on finite elements associated with physical experiments lead to development of new configurations. From the different configurations proposed some stood out. The S-chiral geometric configuration, for example, was described by Meena and Singamneni in their 2020 study. In their research, specimens made of stainless steel 316L were fabricated and subjected to tensile tests in both the x and y directions. They observed a broader range of deformation compared to other metamaterials, and a negative Poisson's ratio was identified. Moreover, the magnitude of the Poisson's ratio was higher in the x-direction. This study serves as an extension of Meena and Signami's work, as the circular shape is a specific instance of the elliptical format. Additionally, the newly proposed metastructure can be utilized as a core for sandwich beams. Figure 1 illustrates a unit cell of this metamaterial, where "a" denotes the horizontal ellipse size, "b" represents the vertical ellipse size, and "t" is the wall thickness. It's important to highlight the use of a unit cell with four ellipses. As depicted, each ellipse in this unit cell possesses a different chirality due to being mirrored. This design is aimed at preventing undesirable mechanical behaviors, such as rotation, when an axial load is applied.

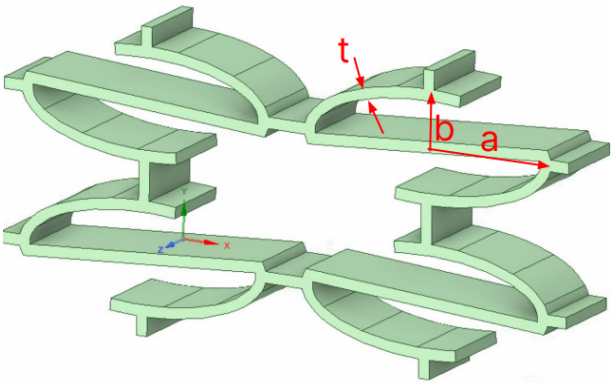

Figure 1. Unit cell of elliptical S-chiral metamaterial for sandwich beam core application.

Chiral meta-structures can be applied as core material for sandwich structures. Their inherent advantages are low density and in-plane and out of plane controllable mechanical properties. Moreover, as discussed by Zhang *et al*. (2022), the key issue on chiral meta-structures is the possibility of making the auxeticity tunable. By manipulating the Poisson ratio, double curvature sandwich structures can be feasible. Therefore, this paper aims to investigate the mechanical behavior of meta-structure, the elliptical S-chiral, as core material for sandwich beams under bending loadings. The objective was to examine the impact of ellipse eccentricity on sandwich flexural properties. To achieve this, numerical simulations were conducted and verified through a single experiment.

2. MATERIALS AND NUMERICAL ANALYSIS

The elliptical S-chiral geometry model proposed is a variation of the model created by Meena and Singamneni (2020). The key difference is the usage of an elliptical shape instead of a circular shape. The elliptical S-chiral configuration will allow not only control the anisotropy at orthogonal axes, but it will be also let to define large variations on Poisson's ratio due to the "empty" spaces between unit cells. Moreover, by changing the elliptical relations between the orthogonal axes and the wall's thickness, it is most likely to tailor the overall meta-structure stiffness.

The primary tool for the elliptical S-chiral metastructure is the finite element analysis. However, to be able perform a non-linear analysis, i.e., polylactic acid (PLA) has an elastic-plastic behavior, a series of tensile tests were done. The additive manufacturing process was used to fabricate the meta-materials specimen. A Creality 5 Plus 3D printer was used. The 1.75 mm diameter PLA filament was deposited by a 0.4 mm nozzle at 80 mm/min. The PLA elastic-plastic behavior was characterized by tensile tests following ASTM D 638 (ASTM D638 2006). Based on experimental data, the multilinear isotropic hardening model from ANSYS is assumed. To be able to perform the elastic-plastic analysis, based on multilinear isotropic hardening, two major information groups must be obtained. For the elastic part, the Young's modulus, the Poisson's ratio and the yield stress must be defined. For the plastic part, the true stress-plastic strain curve must be calculated.

In order to investigate how the S-chiral core behaves under out-of-plane loadings, the ASTM D7250 standard test is employed (ASTM D7250 2020). The sandwich beam configuration is defined by an 8.8 mm core depth, a 64 mm wide circular S-shaped core, and face sheets that are 0.3 mm thick. The wall thickness of the S-chiral core was 1.2 mm, and the entire structure had a total length of 256 mm. The experimental force-displacement curve obtained from the 3-point bending test served as the gold standard for validating the finite element analysis. Figure 2 shows the 3-point bending testing device.

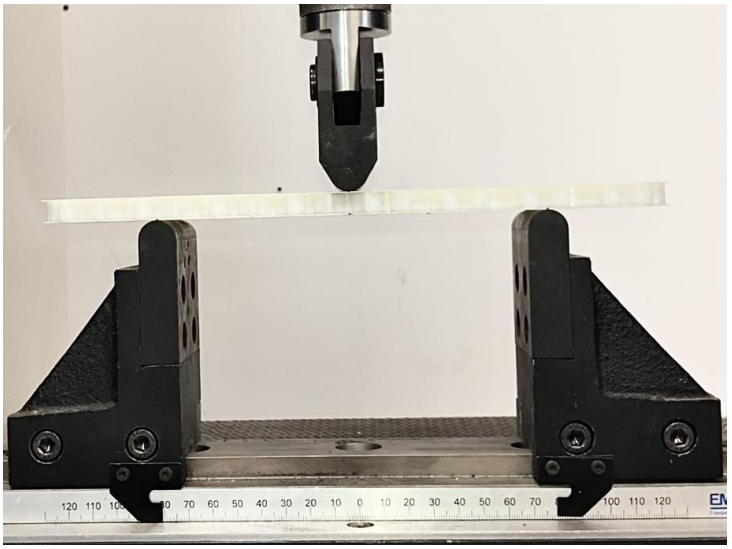

Figure 2. Three-point bending test device of a sandwich beam.

The finite element analysis was performed using ANSYS 2023 R1, research version. Following Paixão and Avila (2023), the same 3D model employed for FEA was fed to the 3D printer slicer code. By applying such a strategy, the consistency between the finite element analysis and the 3D samples manufactured by additive manufacturing is guaranteed.

The finite element analyses were based on C0 class 8-noded brick elements. The sandwich beam differences rely on core configurations. Table 1 summarizes the core configurations simulated by the finite element method. Each unit cell's dimensions depend on the ellipse's geometric aspect ratio, denoted as a/b (horizontal axis/vertical axis). Furthermore, since the sandwich beam dimensions adhere to the ASTM D7250 standard, the number of unit cells in the x and y directions varies. Figure 3 depicts a meshed sample used for the elliptical S-chiral core without the upper sheet, allowing the interior to be visible. The number of degrees of freedom (DOF) is also unique for each group studied.

Table 1. Geometric parameters of sandwich S-shaped metastructures core used in finite element simulations.

Sample	a [mm]	b [mm]	a/b	Unit cells		Degrees-of-freedom
				x-direction	y-direction	(DOF)
1	6.00	6.00	1.00	8	2	343986
2	8.67	6.00	1.44	6	2	306126
3	14.00	6.00	2.33	4	2	291474
4	19.33	6.00	3.22	3	2	277431
5	30.00	6.00	5.00	2	2	267585

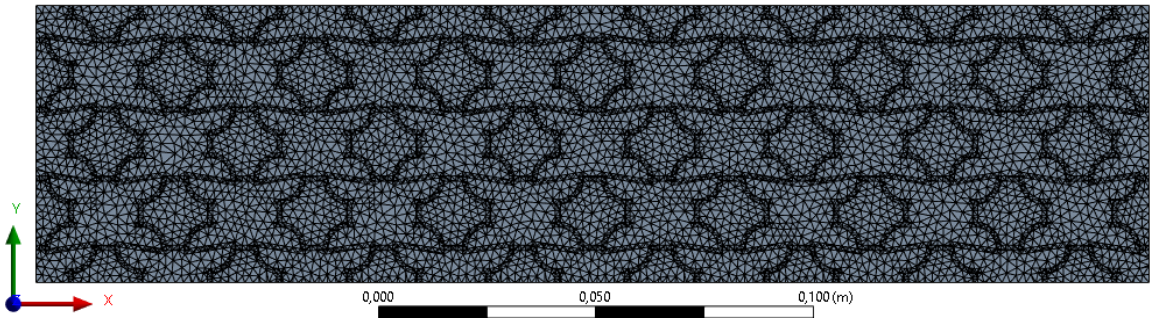

Figure 3. Finite element meshed sample of a sandwich beam with a circular S-shaped core without its upper sheet.

The boundary conditions were relatively straightforward: the lower sheet had two edges constrained with respect to displacement along the z-axis, while movement along the x and y axes was unrestricted. For each sandwich beam simulation, two supporting span lengths were used to compute the flexural properties, as per the recommendations of ASTM D7250. In this case, the spans were set at 160 mm and 150 mm. The experimental setup used for validating the simulations employed a span length of 160 mm. An illustration of this constraint is presented in Figure 4. Additionally, the middle edge of the upper sheet was constrained in its displacement along the x and y directions, while displacements along the z-axis were imposed at the following values: 0.5 mm, 1.0 mm, 1.5 mm, 2.0 mm, 2.5 mm, and 3.0 mm. This simulation's boundary conditions are depicted in Figure 5.

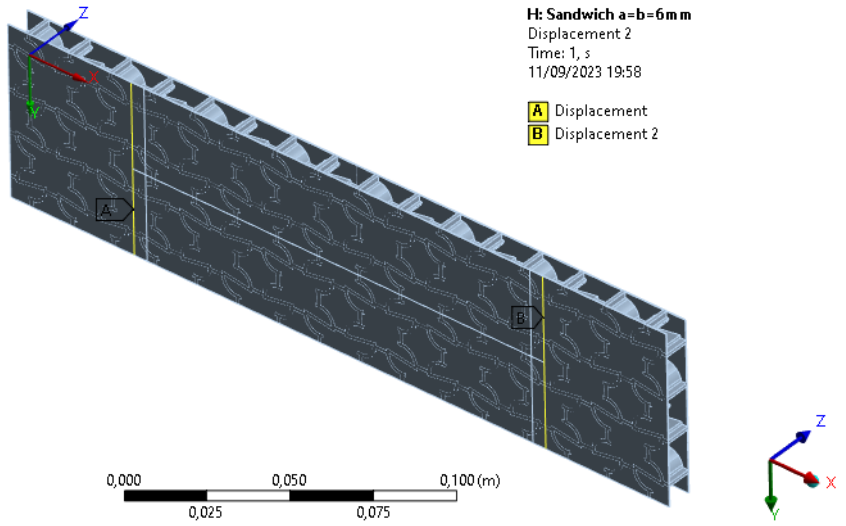

Figure 4. Span constraints used in sandwich beam finite element simulations.

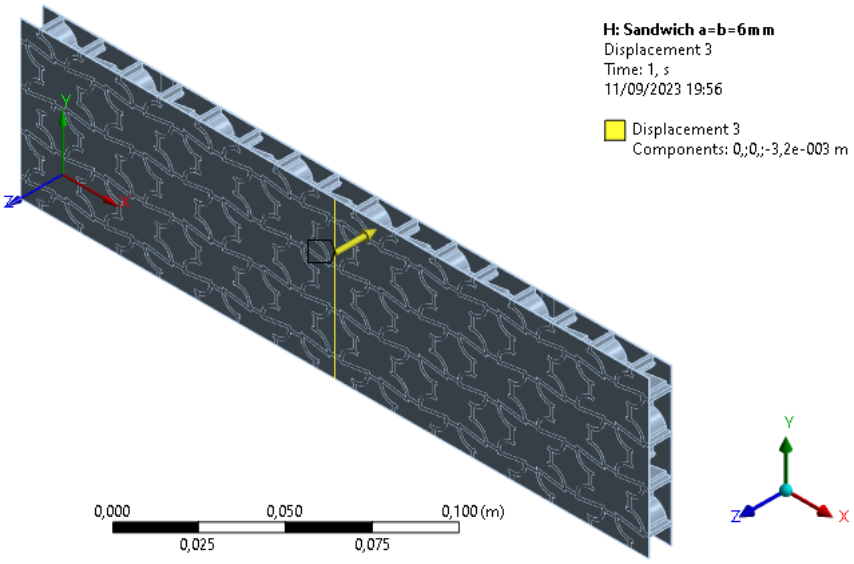

Figure 5. Edge used to apply bending displacement as a boundary condition during flexural testing simulations.

3. RESULTS AND DISCUSSIONS

This section is divided into three parts. The first part pertains to the characterization of raw materials, the second part to the experiment with simulation validation, and the third part contains the results of the sandwich beams' flexural modulus, the core shear modulus and stress profiles obtained during finite element simulations.

3.1 Tensile tests for PLA characterization

Figure 6 describes stress-strain curves obtained based on tensile tests performed following ASTM D638 for PLA characterization. As it can be seen in Fig 6A, the PLA behavior can be considered as elastic-plastic. The plastic region is modeling considering the multilinear isotropic hardening modeling following ANSYS 2023 R1 definition (see Figure 6B). The PLA mechanical properties (linear elastic) obtained are described in Table 2, including the non-linear plastic region (curve approximation) needed for performing an elastic-plastic analysis using ANSYS 2023 R1.

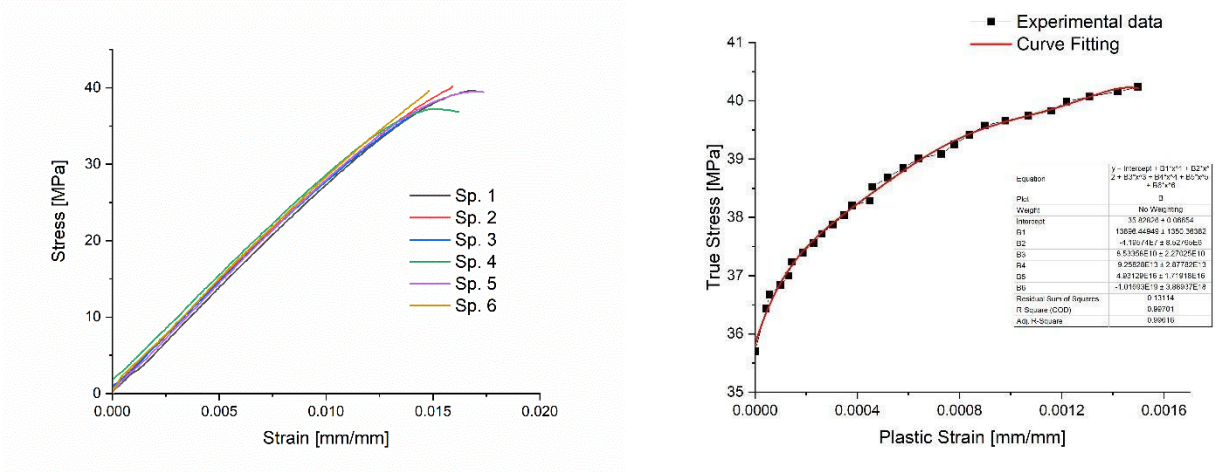

(a) (b)

Figure 6. Tensile test PLA characterization. (a) Stress-strain curve; (b) Plastic region curve.

Table 2. Polyacid lactic (PLA) mechanical properties obtained after tensile tests used in finite element simulations.

Young's modulus (GPa)	**Poisson's ratio**	**Yield stress (MPa)**
2.78 ± 0.08	0.25 ± 0.02	35.70 ± 3.20
Plastic region curve fit: $\sigma_{true}\,[MPa] - \varepsilon_{pl}\,[\text{mm/mm}]$		
$\sigma_{true} = 35.83 + 13896.44\varepsilon_{pl} - 4.19E7\varepsilon_{pl}^{2} + 8.53E10\varepsilon_{pl}^{3} - 9.26E13\varepsilon_{pl}^{4} + 4.93E16\varepsilon_{pl}^{5} - 1.02E19\varepsilon_{pl}^{6}$		

3.2 Experimental bending test and simulation validation

A three-point bending test was conducted using a circular S-shaped core, and data on displacement and force were recorded. The test was carried out at a constant speed of 4.0 mm/min. To validate the simulation results, force reaction values on the edge constraint of the upper plate were obtained for each imposed displacement value. As depicted in Figure 7, the simulation results closely align with the experimental curve. Plastic strain appears to initiate at a 3.2 mm displacement, which explains the slightly higher simulated values at a 3.0 mm displacement. Therefore, it is crucial to collect data within the elastic range when determining flexural properties, taking into consideration only elastic deformation. and numerical results.

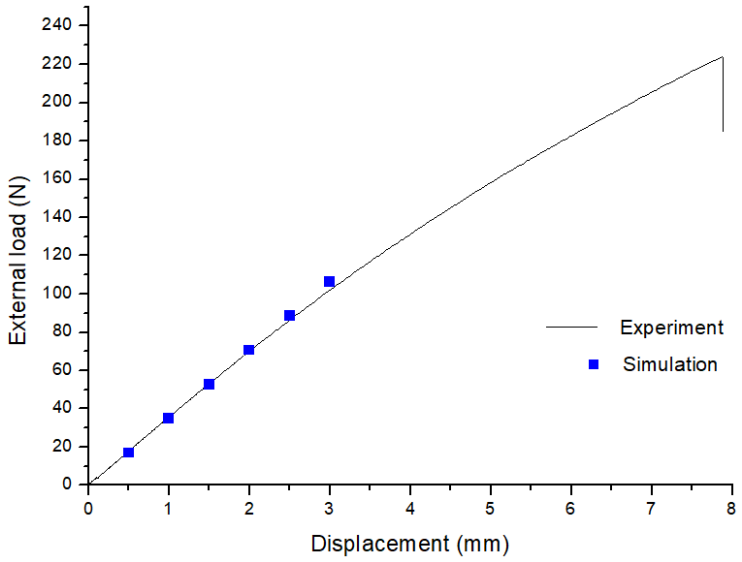

Figure 7. Force dependent on the displacement during experimental bending test of a metastructure sandwich beam and numerical results.

Stress profiles were created to investigate this behavior, and Figure 8 illustrates a directional stress profile along the x-axis of a unit cell situated in the center of the sandwich beam. This region was chosen due to its high stress values. For clarity in the illustration, the upper plate was omitted from the figure. The x-axis stress was analyzed because experimental setups indicated failures stemming from tensile forces in the x-direction. The stress profile reveals that the upper plate experienced the highest stress intensity, indicating a compression failure, with the maximum stress value measuring approximately -35.44 MPa (compression). This observation aligns with the yield stress obtained during the tensile test.

The compression and tension stress fields on the upper and lower sheets, as obtained from the finite element simulations, are consistent with existing literature. Additionally, it is noteworthy that both sheets endure the highest stress values, encompassing both compression and tension. This is an anticipated feature in sandwich structures, where the core's primary role is to increase the separation between the two sheets, thereby enhancing the moment of inertia, flexural stiffness, and overall strength of the sandwich beam (Jones, 1999).

Within the sandwich core, it's noticeable that the stress displays negative values near the upper face, indicating a compressive load on the raw material. The stress intensity diminishes as it penetrates deeper into the material. Near the middle of the depth, the stress approaches null, and the material starts experiencing tensile stress, reaching the maximum tensile stress at the lower sheet. This behavior is typical for materials subjected to flexural loads (Hibbeler, 2004).

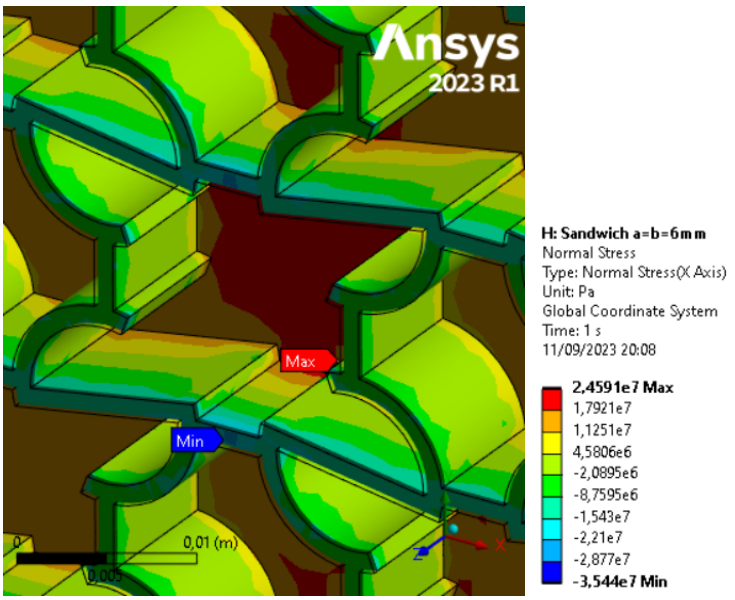

Figure 8. Stress profile in the x-direction of the middle of a sandwich beam subjected to a flexural load without the upper sheet, obtained through finite element simulations.

3.3 Finite element simulation results

The flexural stiffness of five sandwich elliptical S-chiral metastructures was defined through finite element analysis. Figure 9 illustrates the relationship between flexural modulus and the ellipse's aspect ratio (a/b). It was observed that the circular S-shaped core exhibited the lowest flexural stiffness, measuring approximately 3.168 N·m^2. Remarkably, stiffer beams were achieved with greater aspect ratios, with the maximum value observed in the case of the ellipse with a/b = 30/6 (3.566 N·m^2). Additionally, it was noted that a higher ellipse aspect ratio resulted in a smaller sandwich core mass. As a result, all of the elliptical S-chiral metastructures analyzed demonstrated a more favorable ratio between stiffness and mass compared to the circular S-chiral metastructure. This is because the circular geometry exhibited lower stiffness and greater density when compared to the elliptical geometries.

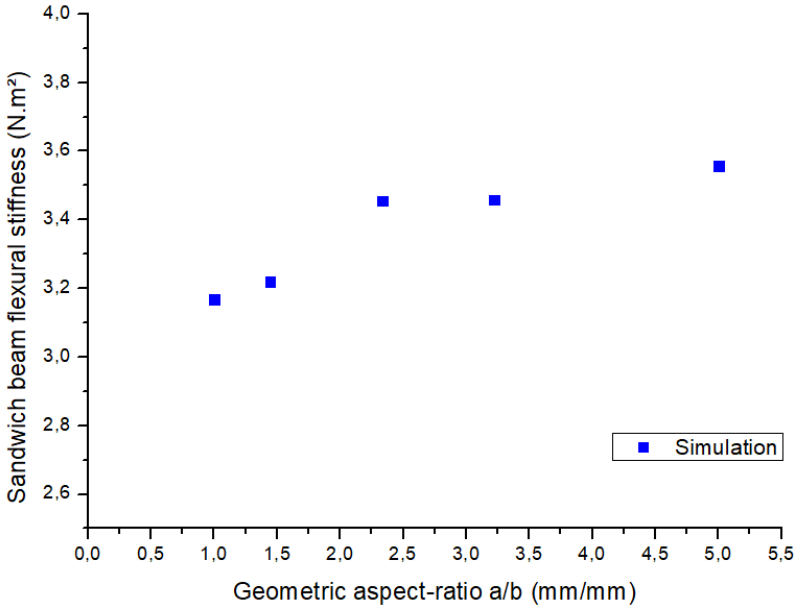

Figure 9. Bending stiffness dependent on the ellipse aspect-ratio obtained through finite element simulations of three points bending tests of sandwich beams made of elliptical S-shaped metastructures cores.

Another crucial elastic property of sandwich beams is the shear modulus of the core. Since the five beams have different ellipse sizes, it was expected that the cores would exhibit varying shear modulus values. The relationship between the core shear modulus and the ellipse aspect ratio is presented in Figure 10. Although one might initially assume that the core shear modulus would increase in tandem with the bending stiffness, this relationship was only observed between the circular core and the one with an aspect ratio of a/b = 8.667/6. The latter core's design allowed for an enhancement in the core shear modulus, even though it was less dense than the circular core. However, the three other ellipses exhibited a decreasing core shear modulus as the aspect ratio increased, in contrast to the earlier observed increase in flexural stiffness.

A question remains: how can it be explained that the sandwich beam bending stiffness is greater while the core is less stiff? As the aspect ratio increases, more material aligns with the beam axis (in this case, the x-direction), contributing to the moment of inertia of the transverse section. However, as the quantity of raw material decreases, it's reasonable to expect that the core shear modulus could also decrease. Thus, the increase in aspect ratio has two factors that act inversely on bending stiffness: the reduction in mass decreases the core shear modulus, contributing to a decrease in stiffness, while the design of the ellipse contributes to an increase in flexural stiffness. Therefore, the resulting bending stiffness depends on the relative influence of each of these two factors in each core design.

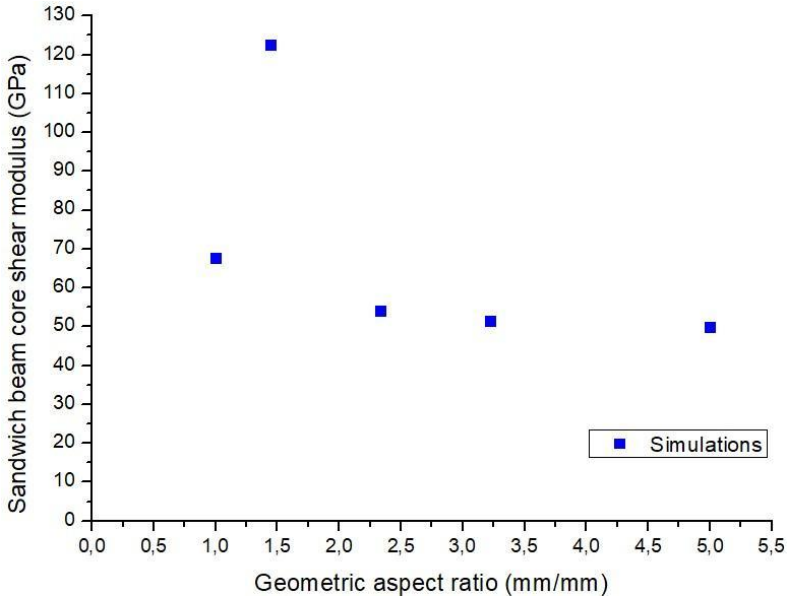

Figure 10. Sandwich beam core shear modulus dependent on the ellipse aspect-ratio obtained through finite element simulations of three points bending tests of sandwich beams made of elliptical S-shaped metastructures cores.

Another intriguing aspect to analyze is the stress profile during the bending test simulations. The normal x-directional stress profile of each of the five-sandwich beam metastructures was generated using the same methodology as the profile already shown for the circular case used to validate the failure mode. However, we employed a smaller deflection to ensure that the structures were subjected only to elastic strains. Figures 11-15 display the normal x-direction stress profile of the unit cell at the center of each sandwich beam, without the upper sheet, during a three-point bending test simulation with a deflection of 1.5 mm and a span length of 160 mm.

For all the beams, it is evident that the maximum stress occurred near the center of the lower sheet and the minimum stress near the center of the upper sheet. This behavior is expected in beam structures, as discussed during the explanation of the circular S-shaped stress profile used for failure validation. It can be inferred that there is very little difference between the values of maximum and minimum stress, preventing the establishment of any relationship between the elliptical aspect ratio of the cores and the stress values. This is intriguing because structures with greater flexural stiffness, as reported in this work and typically less dense, exhibit a similar stress distribution and might consequently display similar flexural strength. It's important to remember that greater stiffness also helps reduce the maximum deflection, which is a crucial parameter to consider in beam structures.

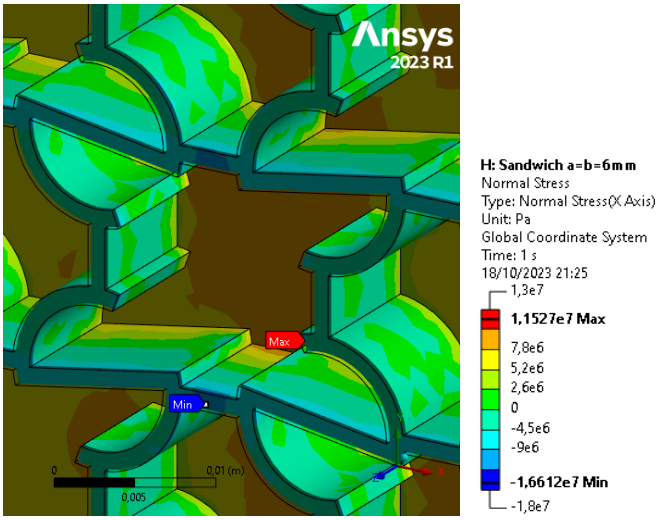

Figure 11. Normal stress profile in the x-direction of a sandwich beam metastructure with an elliptical S-shaped core (a=b=6mm) during a three-point bending test simulation with 1.5 mm deflection.

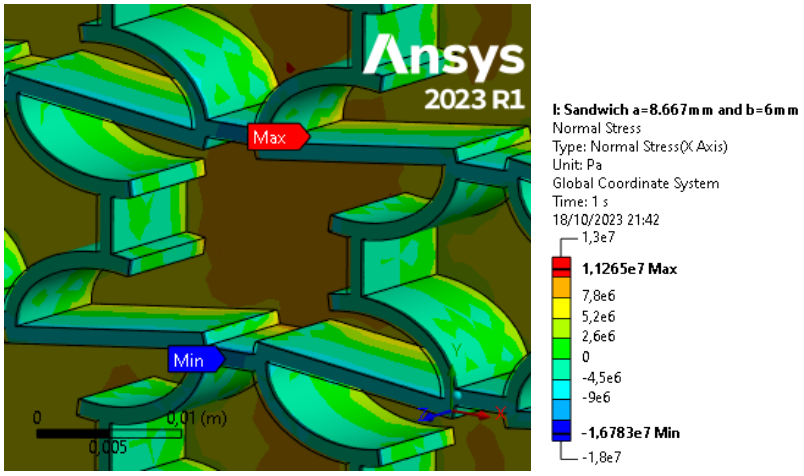

Figure 12. Normal stress profile in the x-direction of a sandwich beam metastructure with an elliptical S-shaped core (a=8.667mm, b=6mm) during a three-point bending test simulation with 1.5 mm deflection.

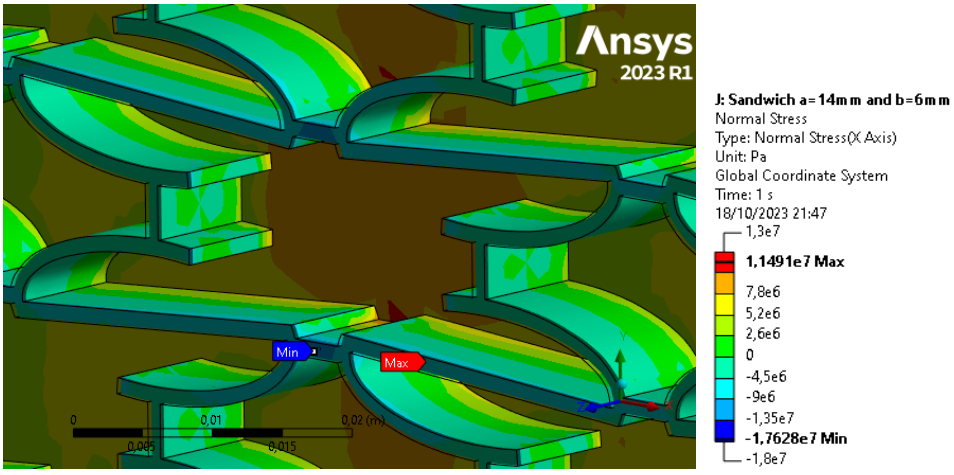

Figure 13. Normal stress profile in the x-direction of a sandwich beam metastructure with an elliptical S-shaped core (a=14mm, b=6mm) during a three-point bending test simulation with 1.5 mm deflection.

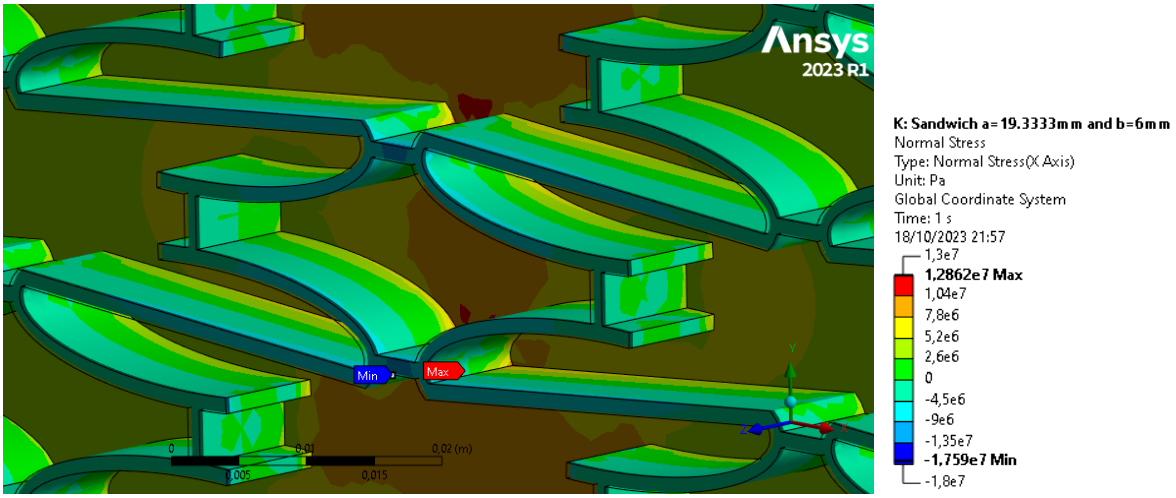

Figure 14. Normal stress profile in the x-direction of a sandwich beam metastructure with an elliptical S-shaped core (a=19.3333mm, b=6mm) during a three-point bending test simulation with 1.5 mm deflection.

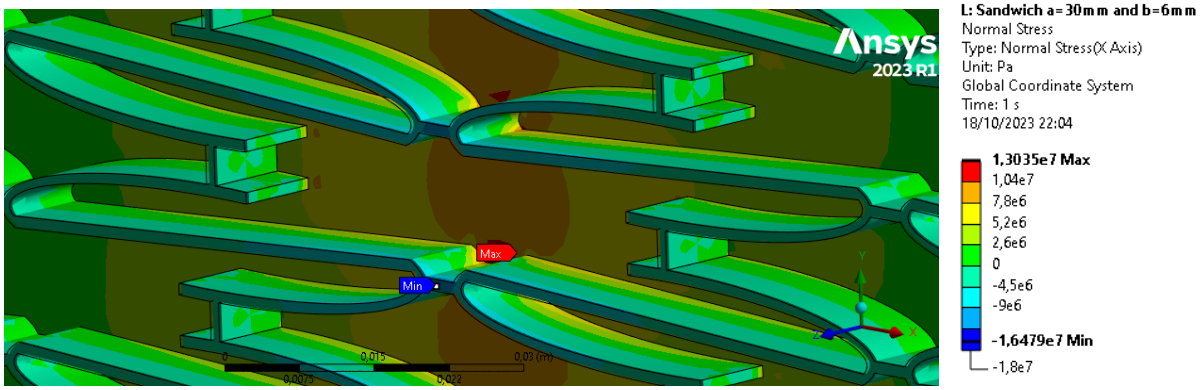

Figure 15. Normal stress profile in the x-direction of a sandwich beam metastructure with an elliptical S-shaped core (a=30mm, b=6mm) during a three-point bending test simulation with 1.5 mm deflection.

4. CONCLUSIONS REMARKS

The objective of this study was to determine the flexural elastic properties of a family of sandwich beams with cores consisting of elliptical S-shaped metastructures through finite element analyses. The simulations were validated using experimental data of force and displacement obtained from a three-point bending test performed on a sandwich structure with a circular S-shaped metastructure core. To conclude this work, the following key points are worth noting:

1. The circular S-shaped metastructure core exhibits the lowest flexural stiffness, approximately 3.168 N·m².
2. The highest flexural stiffness for the sandwich beam was achieved with a core having the greatest ellipse aspect ratio, with a/b = 30/6, measuring 3.566 N·m².
3. Increasing the ellipse aspect ratio (a/b) leads to an increase in sandwich beam flexural stiffness. This is noteworthy because as the ellipse size grows, the core mass decreases.
4. Elliptical geometries show higher flexural modulus values and are less dense compared to the circular geometry. Consequently, sandwich beams with metamaterial cores, specifically S-elliptical cores, offer the advantage of reduced mass while maintaining acceptable stiffness levels.
5. The highest core shear modulus value was not achieved with the ellipse having the greatest aspect ratio, but with the second eccentricity at a/b = 8.667/6. After this point, there was a decrease in core shear modulus observed as the ellipse aspect ratio increased.
6. The seemingly counterintuitive relationship between increasing aspect ratio enhancing sandwich beam flexural stiffness while core shear modulus decreases can be explained by the design's contribution in increasing the core's moment of inertia.
7. The analysis of normal stress profiles in the x-direction revealed no significant differences between the structures. This suggests that it is possible to achieve a stiffer sandwich beam with less mass and potentially similar strength by increasing the ellipse aspect ratio of the cellular core.

5. ACKNOWLEDGEMENTS

The authors would like to acknowledge the financial support provided by the Brazilian Research Council (CNPq) under grants 406040/2021-4, 307385/2022-1 and the Coordenação de Aperfeiçoamento do Pessoal do Ensino Superior (CAPES) under grant 001.

6. REFERENCES

Alderson A., Alderson K.L., Attard D, *et al.* (2010) Elastic constants of 3-, 4- and 6-connected chiral and anti-chiral honeycombs subject to uniaxial in-plane loading. Compos Sci Technol 70:1042–1048. https://doi.org/10.1016/j.compscitech.2009.07.009

ASTM D 7250 (2020) Standard Practice for Determining Sandwich Beam Flexural and Shear Stiffness. D7250. ASTM Int 1–12. https://doi.org/10.1520/D7250-20.2

ASTM D 638 (2006) Standard Test Method for Tensile Properties of Plastics 1. ASTM Int 1–15. https://doi.org/10.1520/D0638-22.1

Francisco M.B., Pereira J.L.J., Oliver G.A., *et al.* (2022) A review on the energy absorption response and structural applications of auxetic structures. Mech Adv Mater Struct 29:5823–5842. https://doi.org/10.1080/15376494.2021.1966143

Hibbeler, R.C. *Resistência dos materiais*. São Paulo: Pearson Prentice Hall, 2004.

Jones, R.. *Mechanics of Composite Materials*. New York: Taylor & Francis, 1999.

Liu Y., Zhang X. (2011) Metamaterials: A new frontier of science and technology. Chem Soc Rev 40:2494–2507. https://doi.org/10.1039/c0cs00184h

Masters I.G., Evans K.E. (1996) Models for the elastic deformation of honeycombs. Compos Struct 35:403–422. https://doi.org/10.1016/S0263-8223(96)00054-2

Meena, K., & Singamneni, S. (2020). Investigation of a novel chiral S-shaped auxetic structure under large tensile deformation. Physica Status Solidi B, 257(11), 2000239. https://doi.org/10.1002/pssb.202000239

Montgomery-Liljeroth E., Schievano S., Burriesci G. (2023) Elastic properties of 2D auxetic honeycomb structures- a review. Appl Mater Today 30:101722. https://doi.org/10.1016/j.apmt.2022.101722

Mousanezhad D., Haghpanah B., Ghosh R., *et al.* (2016) Elastic properties of chiral, anti-chiral, and hierarchical honeycombs: A simple energy-based approach. Theor Appl Mech Lett 6:81–96. https://doi.org/10.1016/j.taml.2016.02.004

Paixão N.M.M., Ávila A.F. (2023) Finite element simulations of auxetic structure combined with honeycomb using unidirectional continuous carbon fiber composite properties. J Eng Exact Sci 9:15430–01e. https://doi.org/10.18540/jcecvl9iss1pp15430-01e

Shukla S., Behera B.K. (2022) Auxetic fibrous structures and their composites: A review. Compos Struct 290:115530. https://doi.org/10.1016/j.compstruct.2022.115530

Wang T., Wang L., Ma Z., Hulbert G.M. (2018) Elastic analysis of auxetic cellular structure consisting of re-entrant hexagonal cells using a strain-based expansion homogenization method. Mater Des 160:284–293. https://doi.org/10.1016/j.matdes.2018.09.013

Zhang J., Lu G., You Z. (2020) Large deformation and energy absorption of additively manufactured auxetic materials and structures: A review. Compos Part B Eng 201:108340. https://doi.org/10.1016/j.compositesb.2020.108340

Zhang X.Y., Ren X., Zhang Y., Xie Y.M. (2022) A novel auxetic metamaterial with enhanced mechanical properties and tunable auxeticity. Thin-Walled Struct 174:109162. https://doi.org/10.1016/j.tws.2022.109162

7. RESPONSIBILITY NOTICE

The first and the last author are the only responsible for the printed material included in this paper.